



Actual Crop Evapotranspiration Estimation of Wheat Crop Using SEBAL Algorithm and Remotely Sensed Data

Manju Dhruw^{a++*}, V. K. Pandey^{b#} and Shruti Verma^{a†}

^a Department of Soil and Water Engineering, SVCAET & RS, Indira Gandhi Krishi Vishvavidyalya, Raipur, (Chhattisgarh), India.

^b SVCAET & RS, Indira Gandhi Krishi Vishvavidyalya, Raipur, (Chhattisgarh), India.

Authors' contributions

This work was carried out in collaboration among all authors. All authors read and approved the final manuscript.

Article Information

DOI: 10.9734/CJAST/2023/v42i204150

Open Peer Review History:

This journal follows the Advanced Open Peer Review policy. Identity of the Reviewers, Editor(s) and additional Reviewers, peer review comments, different versions of the manuscript, comments of the editors, etc are available here: <https://www.sdiarticle5.com/review-history/103419>

Original Research Article

Received: 11/05/2023

Accepted: 13/07/2023

Published: 14/07/2023

ABSTRACT

Estimation of evapotranspiration is imperative for effective forest, irrigation and water resources management as well as to increase yields and for better crop management. This study aims to evaluate the effectiveness of the Surface Energy Balance Algorithm for Land (SEBAL) in estimating actual evapotranspiration for 15 years of wheat crop in the 2A distributary of Mahanadi canal Command which is situated in Dhamtari district of Chhattisgarh state of India. The Landsat 7 and 8 satellite images from February – March (2007 -2021) were used to acquire the coefficients of the respective bands. To validate the outcomes from the SEBAL algorithm, FAO Penman-Monteith

⁺⁺ Ph.D. Scholar;

[#] Head (SWE) and Dean;

[†] Junior Research Fellow under National Hydrology Project;

*Corresponding author: E-mail: manjudhruw26@gmail.com;

methods were employed to calculate the evapotranspiration values and evaluated using suitable performance metrics. The evaluation using SEBAL, along with the FAO-Penman–Monteith method, showed that SEBAL has a sufficient accuracy for estimating ET. The results showed that the SEBAL generated evapotranspiration values are in high agreement with the FAO Penman-Monteith method registering the highest correlation value ($R^2 = 0.826$) and the corresponding Root Mean Square Error was (RSME = 0.4386), Normalized Root Mean Square, (NRMSE= 0.386), Mean Absolute Error (MAE=1.17) and Nash Sutcliffe Efficiency(ENS = 0.843) for wheat crop. In 2010 maximum ET_c and in 2021 minimum ET_c of wheat crop in the study area. The outcomes show that since the performance of the SEBAL algorithm in estimating the actual evapotranspiration using Landsat 7 and 8 satellite images is acceptable, the SEBAL algorithm could be a very convenient method. Moreover, it could easily be assimilated into farming management systems and precision agriculture for better decision-making and higher yield.

Keywords: Remote sensing; GIS; SEBAL algorithm; thermal band; FAO penman- monteith.

1. INTRODUCTION

Over the last few decades with the reduction of water resources, India is facing critical problems with industrial and agricultural growth being impacted. In agriculture, water requirements are associated with irrigation water use. Prediction of irrigation water demand involves computation of many water balance factors, and evapotranspiration (ET) is one of its major components. ET is the combined loss of water from the soil as well as plants and it is a crucial component of the hydrologic cycle. It is difficult to consider these two processes separately since they occur almost simultaneously at varied rates with high spatial variability [1]. As a result, evapotranspiration estimates are important for hydrology, irrigation, forest and water resources management. The evapotranspiration drives the soil water-energy balance which is largely used in general circulation models and climate modelling. Consequently, river water flow forecasting, crop yield forecasting, irrigation management systems, river/ lake water quality are all dependent on evapotranspiration levels [2-5]. For this reason, it is essential to accurately estimate the water budget [6,7]. Better and accurate evapotranspiration estimates would allow for effective irrigation planning and optimal water usage for other agricultural purposes [8]. The evapotranspiration rate depends on many factors such as temperature, solar radiation, humidity, wind and vegetation [1]. Essentially, the reference evapotranspiration (ET_0) is calculated using techniques such as FAO Penman and Hargreaves methods or measured directly using a lysimeter [9]. So far, various methods have been developed including direct/field measurements and empirical equations for estimating evapotranspiration. However, ET_0 consists of a complex and nonlinear structure

requiring multiple parameters for estimation [10]. This nonlinear and multi-parameter nature makes estimation methods tedious and time-consuming [11]. The disadvantage of the conventional method is that it can only provide accurate evapotranspiration assessments of a homogeneous region provided a meteorological gauge station is in the vicinity. Another drawback is that ET_0 cannot be extrapolated to different sites.

Consequently, surface observation networks have been developed, yet it is not possible to make meteorological measurements at all places covering large areas. The meteorological observations do not provide true spatial evapotranspiration of an area [3] (Liu et al. 2011; Antonopoulos and Antonopoulos 2017). On the other hand, remote sensing techniques allow for filling in the gap in providing the much-needed spatially observed data [12]. The advancements in remote sensing techniques in recent years together with the accessibility to satellite images have allowed for alternative and reliable methods for evapotranspiration estimations at regional scales (Mao and Wang 2017). Evapotranspiration models based on remote sensing provide relatively accurate estimations of evapotranspiration in large areas with minimal use of terrestrial data [3].

Numerous models have been developed to estimate evapotranspiration using remote sensing methods. Out of all the proposed models for estimating evapotranspiration [13], the Surface Energy Balance Algorithm for Land (SEBAL) model has proven to be the most widely used amongst researchers in over 30 countries. This model was developed by Bastiaanssen and improved by Allen [3]. The SEBAL model has proven to estimate evapotranspiration with better

accuracy. Its registered accuracies of 85% at a farm scale while more than 95% accuracy has been recorded on a regional scale [14].

All these studies prove the efficiency and accuracy of the SEBAL method in estimating evapotranspiration across different geographical areas, climates, and land cover conditions. The SEBAL model has a lot of merits making it useful for such applications. It uses a linear relationship between the earth's surface temperature and near-surface vertical temperature gradients selected by cold and dry pixels [3]. More importantly, the SEBAL algorithm needs little information from the incoming terrestrial data to calculate the actual evapotranspiration in each pixel and can further estimate evapotranspiration for large areas [15] making it advantageous for real-life farm-based applications. Despite a number of studies being performed with SEBAL algorithms in evapotranspiration, improvements in accuracy are required for better results. In addition, the SEBAL method has a lower

sensitivity to meteorological inputs and could easily be used in areas with fewer meteorological stations. According to studies done so far, it is necessary to evaluate and verify evapotranspiration estimates for each environmental condition and agricultural field since limited research has been carried out in the area of satellite estimates of evapotranspiration of crops [16].

2. MATERIALS AND METHODS

2.1 Study Area

2A Distributary lies between $20^{\circ} 42'04''$ and $21^{\circ} 29'29''$ N latitudes and $81^{\circ} 47'50''$ and $81^{\circ} 85'30''$ E longitudes. The geographical area of the distributary 2A was 200.05 KM^2 with a Cultivable Command Area (C.C.A) of 12461.58 ha. The major crop of the area is paddy in the Kharif season and in the Rabi season mostly summer paddy and wheat, chickpea, pulses (mainly gram and millets) and oil seeds are grown.

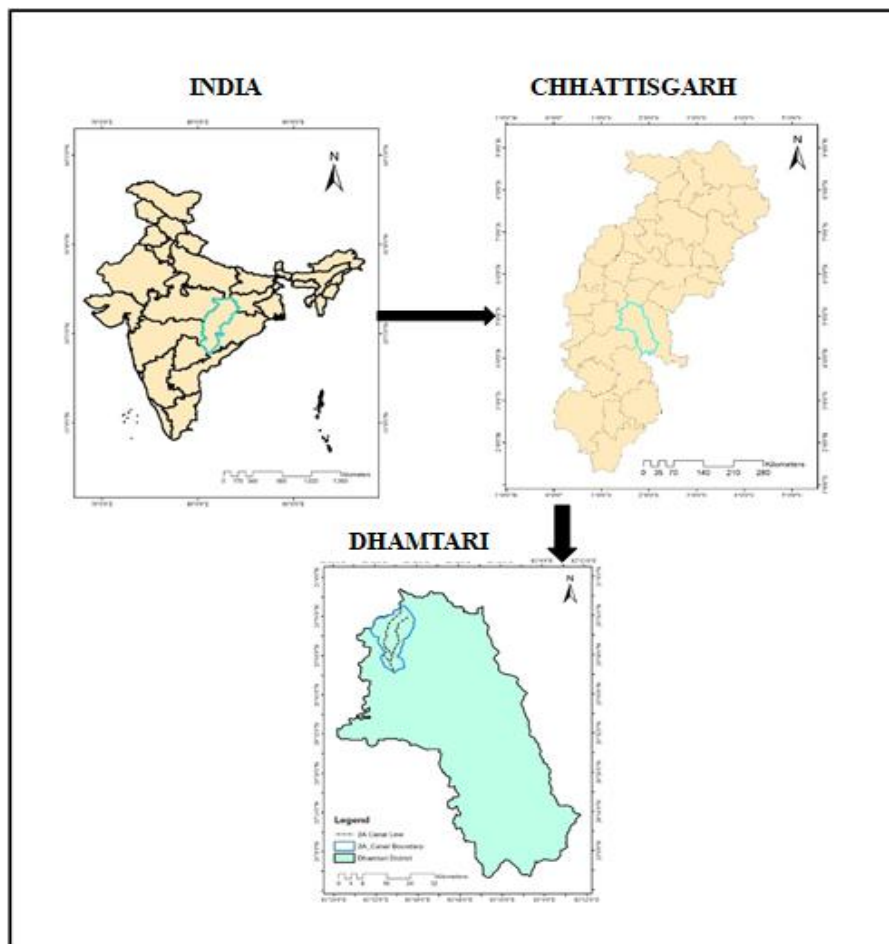


Fig. 1. Location map of the study area

2.2 Methodology

The Landsat 7 and 8 satellite images from February – March (2007 -2021) were used to acquire the coefficients of the respective bands.

15 years data were used for this study area. In this study, daily and hourly meteorological data from 2007-2021 were used. The data included minimum and maximum humidity, average wind speed and sun hours.

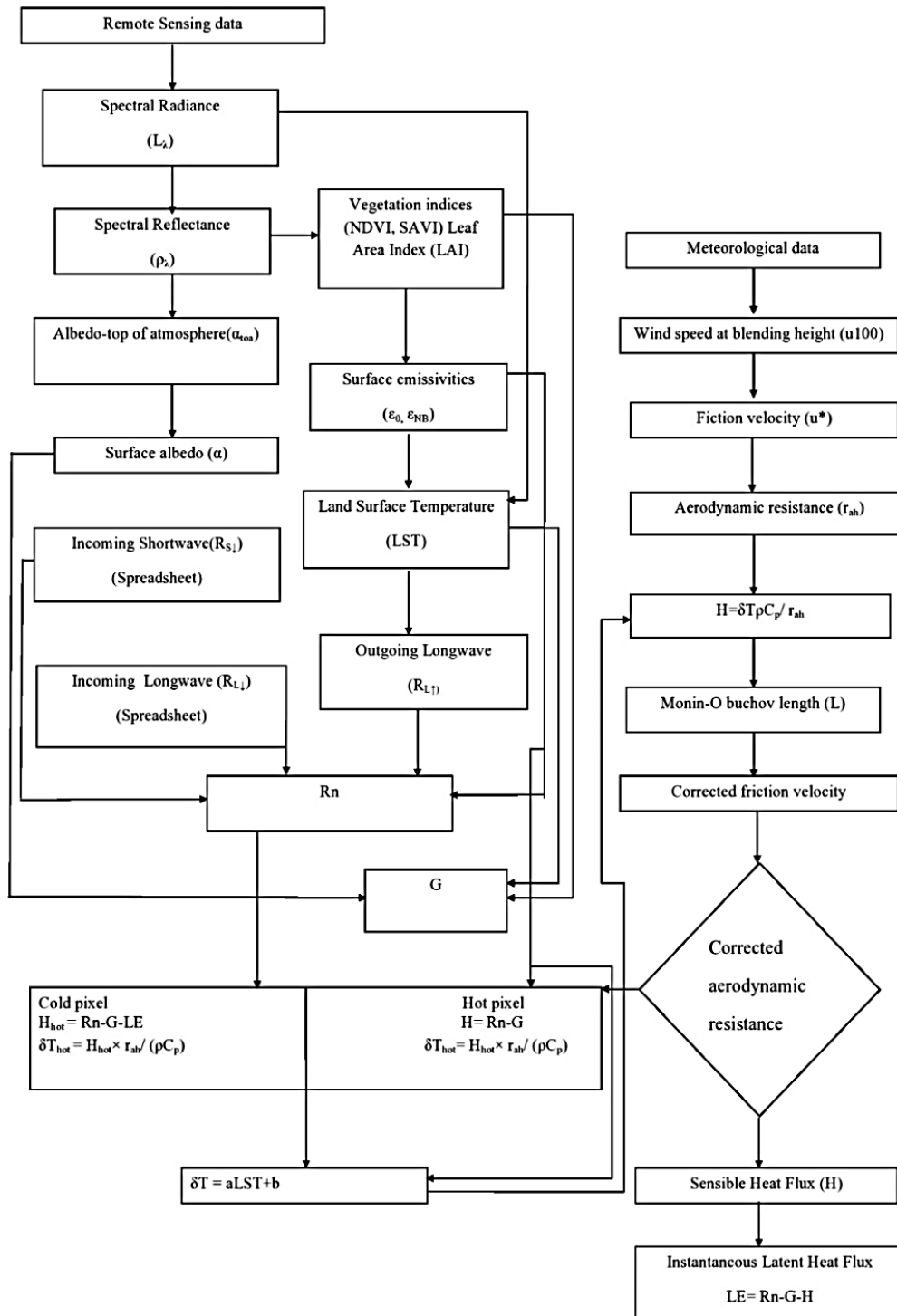


Fig. 2. Flow chart of the computational steps of SEBAL algorithm (Bezerrz et al. 2015)

2.3 Surface Energy Budget Equation

The total solar energy coming from the sun and atmosphere in the form of long and shortwave radiation is transformed and utilized for (a) soil heating, (b) surface environment heating (sensible heat flux to the atmosphere), and (c) transforming water into vapour (latent heat flux from the crop or soil surfaces). All the energy involved in the soil vegetation atmosphere interface can be given as the Energy Balance equation. The actual ET was obtained using the surface energy balance equation:

$$\lambda ET = R_n - G - H \quad (1)$$

Where, R_n is the net radiation at the surface (W/m^2), G is the soil heat flux (W/m^2), H is the sensible heat flux to the air (W/m^2), ET is the latent heat flux associated with ET (instantaneous value for the time of the satellite overpass, W/m^2).

2.4 Description of SEBAL Algorithm

The key input data for SEBAL consists of spectral radiance in the visible, near-infrared and thermal infrared part of the spectrum. In addition to satellite images, the SEBAL model requires routine weather data parameters (wind speed, humidity, solar radiation and air temperature).

2.5 Net Radiation (R_n)

The net radiation flux at the surface (R_n) represents the actual radiant energy available at the surface. It is computed by subtracting all outgoing radiant fluxes from all incoming radiant fluxes, which can be expressed as:-

$$R_n = (1-\alpha)RS_{\downarrow} + R_{L\downarrow} - R_{L\uparrow} - (1-\epsilon_0)R_{L\downarrow} \quad (2)$$

Where RS_{\downarrow} is the incoming shortwave radiation (W/m^2), α is the surface albedo (dimensionless), $R_{L\downarrow}$ is the incoming long wave radiation (W/m^2), $R_{L\uparrow}$ is the outgoing long wave radiation (W/m^2), and ϵ_0 is the surface thermal emissivity (dimensionless) (Water set al. 2002).

2.6 Surface Albedo (α)

Surface albedo (α) is defined as the ratio of the reflected radiation to the incident short wave radiation. On Surface it is a reflection coefficient. The albedo at the top of the atmosphere (α_{toa}) was computed. This is the albedo unadjusted for

atmospheric transmissivity and is computed as follows:

$$\alpha_{toa} = \sum(\omega_{\lambda} \times \rho_{\lambda}) \quad (3)$$

Where, ρ_{λ} is the computed reflectivity and ω_{λ} is a weighting coefficient for each band computed as follows:

$$\omega_{\lambda} = \frac{ESUN_{\lambda}}{\sum ESUN_{\lambda}} \quad (4)$$

Where $ESUN$ is elevation of the sun. Albedo is defined as the ratio of the electromagnetic radiation reflected from the surface of the soil and the plant to the incident light emitted by the sun. Surface albedo is computed by correcting the α_{toa} for atmospheric transmissivity:

$$\alpha = \frac{\alpha_{toa} - \alpha_{path_radiance}}{\tau_{sw}^2} \quad (5)$$

Values for $\alpha_{path_radiance}$ range between 0.025 and 0.04 and for SEBAL we recommend a value of 0.35 based on Bastiaanssen (1998). τ_{sw} includes the transmissivity of both direct solar beam radiation and diffuse (scattered) radiation to the surface. We calculate τ_{sw} assuming clear sky and relatively dry conditions using an elevation-based relationship from FAO-56:

$$\tau_{sw} = 0.75 \times 2 \times 10^{-5} \times z \quad (6)$$

Where, z is the elevation above sea level (m).

2.7 Incoming Shortwave Radiation (R_n)

Incoming shortwave radiation is the direct and diffuse solar radiation flux that actually reaches the earth's surface (W/m^2). Its value is computed as follows:

$$R_{s\downarrow} = G_{sc} \times \cos \theta \times d_r \times \tau_{sw} \quad (7)$$

Where,

G_{sc} is the solar constant ($1367 W/m^2$),
 $\cos \theta$ is the cosine of the solar incidence angle
 d_r is the inverse squared relative earth-sun distance
 τ_{sw} is the atmospheric transmissivity.

$$d_r = 1 + 0.033 \cos \left(DOY \frac{2\pi}{365} \right) \quad (8)$$

d_r can be calculated as Solar incidence ($\theta = 90^\circ - \text{sun elevation angle}$) Atmospheric transmissivity z is the elevation above sea level (m)

2.8 Outgoing Long wave Radiation (RL)

The outgoing long wave radiation is the thermal radiation flux emitted from the earth's surface to the atmosphere (W/m^2). It is computed in SEBAL through the following

Steps

Computation of vegetation indices of Normalized Difference Vegetation Index (NDVI), Soil Adjusted Vegetation Index (SAVI), and Leaf Area Index (LAI). The NDVI is the ratio of the differences in reflectivities for the near-infrared band (5) and the red band (4) to their sum for landsat-8 and for landsat -7 the near-infrared band (4) and the red band (3) to their sum:

$$NDVI = (R_1 - R_2)/(R_1 + R_2) \quad (9)$$

The NDVI is a sensitive indicator of the amount and condition of green vegetation. Values for NDVI range between -1 and +1. Green surfaces have a NDVI between 0 and 1 and water and cloud are usually less than zero.

The SAVI is an index that attempts to "subtract" the effects of background soil from NDVI so that impacts of soil wetness are reduced in the index. It is computed as:

$$SAVI = (1 + L)(R_1 - R_2)/(R_1 + R_2) \quad (10)$$

Where; L is a constant for SAVI. If L is zero, SAVI becomes equal to NDVI. A value of 0.5 frequently appears in the literature for L. The LAI is the ratio of the total area of all leaves on a plant to the ground area represented by the plant. It is an indicator of biomass and canopy resistance. LAI is computed for southern Idaho using the following empirical equation:

$$LAI = \frac{1n\left(\frac{0.69 - SAVI}{0.59}\right)}{0.91} \quad (11)$$

Where; $SAVI_{ID}$ is the SAVI calculated from Equation (11)

1. Computation of Surface emissivity (ϵ)

Surface emissivity (ϵ) is the ratio of the thermal energy radiated by the surface to the thermal

energy radiated by a blackbody at the same temperature.

2. Computation of Outgoing Long wave Radiation ($R_{L\uparrow}$) This is computed using the Stefan-Boltzmann equation:

$$R_{L\uparrow} = \epsilon_0 \times \sigma \times T_s^4 \quad (12)$$

Where ϵ_0 is the "broad-band" surface emissivity (dimensionless), σ is the Stefan-Boltzmann constant ($5.67 \times 10^{-8} W/m^2/K^4$), and T_s is the surface temperature (K).

2.9 Choosing the "Hot" and "Cold" Pixels

The "cold" pixel is selected as a wet, well-irrigated crop surface having full ground cover by vegetation. The surface temperature and near-surface air temperature are assumed similar at this pixel. The "hot" pixel is selected as a dry, bare agricultural field where ET is assumed zero.

2.10 Incoming Long Wave Radiation ($R_{L\downarrow}$)

The incoming long wave radiation is the downward thermal radiation flux from the atmosphere (W/m^2). It is computed using the Stefan-Boltzmann equation:

$$R_{L\downarrow} = \epsilon_0 \times \sigma \times T_s^4 \quad (13)$$

Net surface radiation (R_n) is calculated using Equation (3.4)

2.11 Calculate Land Surface Temperature (LST)

For Landsat-7: This technique can only be used to process Landsat-7 (band 6) is used respectively.

Below given formula used to calculate:-

$$L\lambda = ((LMAX\lambda - LMIN\lambda)/(QCALMAX - QCALMIN)) \times (QCAL - QCALMIN) + LMIN\lambda \quad (14)$$

Where,

$L\lambda$ = Spectral Radiance (watts/meter)

QCAL= Quantized calibrated pixel value in DN

$LMAX\lambda$ = Spectral Radiance scaled to QCAL MAX (watts/meter)

$LMIN\lambda$ = Spectral Radiance scaled to QCAL MIN (watts/meter)

QCALMAX = Maximum Quantized calibrated pixel value (corresponding to $LMAX\lambda$) in DN

QCALMIN = Minimum Quantized calibrated pixel value (corresponding to LMIN_λ) in DN

For Landsat-8: This technique can only be used to process Landsat-7 (band 6) and Landsat-8 data (band 10) is used respectively to estimate brightness temperature band (4-3) for Landsat-7 and band (5-4) for Landsat-8 are used to calculate NDVI.

Below given formula used to calculate :-

$$L\lambda = \frac{(L_{max}-L_{min}) \times Q_{cal}}{(Q_{calmax}-Q_{calmin})} + L_{min} - Q_i \quad (15)$$

Where,

L_{max} is the maximum radiance ($Wm^{-2}sr^{-1}\mu m^{-1}$)

L_{min} is the minimum radiance ($Wm^{-2}sr^{-1}\mu m^{-1}$)

Q_{cal} is the DN value of pixel

Q_{cal max} is the maximum DN value of pixels

Q_{cal min} is the minimum DN value of pixels

O_i is the correction value for band 10

2.12 Soil Heat Flux (G)

Soil heat flux is the rate of heat storage into the soil and vegetation due to conduction. Estimates of G/R_n for agriculture surfaces are between 0.05–0.15.

$$\frac{G}{R_n} = \frac{T_s}{\alpha} \times [0.0032 \times \alpha + 0.0062 \times \alpha^2] \times [1 - 0.978 \times NDVI^4] \quad (16)$$

2.13 Sensible Heat Flux (H)

Sensible heat flux is the rate of heat loss to the air by convection and conduction, due to a temperature difference. It is compute using the following equation for heat transport:

$$H = \frac{D \times CD \times dt}{rah} = \rho \times C_p \times dt/rah \quad (17)$$

Where

ρ is air density (kg/m³),

C_p is air specific heat (1004 J/kg/K),

dT (K) is the temperature difference (T₁ - T₂) between two heights (z₁ and z₂),

rah is the aerodynamic resistance to heat transport (s/m).

Latent Heat Flux (λET), Instantaneous ET (ET_{inst}), and Reference ET Fraction (ET_rF) computation Latent heat flux is the rate of latent heat loss from the surface due to

evapotranspiration. It can be computed for each pixel using the following Equation:

$$\lambda ET = R_n - G - H \quad (18)$$

Where

λET is an instantaneous value for the time of the satellite overpass (W/m²).

An instantaneous value of ET in equivalent evaporation depth is computed as:

$$ET_{inst} = 3600 \times \frac{\lambda ET}{\lambda} \quad (19)$$

Where

ET_{inst} is the instantaneous ET (mm/hr), 3600 is the time conversion from seconds to hours,

λ is the latent heat of vaporization or the heat absorbed when a kilogram of water evaporates (J/kg) is computed as:

$$\lambda = [2.501 - 0.00236(TS - 273)] \times 10^6 \quad (20)$$

2.14 Reference ET Fraction

The Reference ET Fraction (ET_rF) is defined as the ratio of the computed instantaneous ET (ET_{inst}) for each pixel to the reference ET (ET_r) computed from weather data:

$$ET_r F = \frac{ET_{inst}}{ET_r} \quad (21)$$

Daily values of ET (ET₂₄) are often more useful than instantaneous ET.

2.15 Seasonal Evapotranspiration (ET_{seasonal})

A seasonal evapotranspiration map was derived from the 24-hour evapotranspiration data by extrapolating the ET₂₄ proportionally to the reference evapotranspiration (ET_r). ET_r is computed for a specific location and therefore does not represent the actual condition at each pixel. However, since ET_r is used only as an index of the relative change in weather, and therefore ET, for the image area. The ET_rF computed for the time of the image is constant for the entire period represented by the image. The length of the season for which ET is desired will be decided based on the period represented by each satellite image within the chosen season. The cumulative ET_r for the period represented by the image was computed by summing of daily ET_r values over the period as explained below :-

$$ET_{24} = ET_r F \times ET_{r-24} \quad (22)$$

Where; ET_{r-24} is the cumulative 24-hour ET_r for the day image. This is calculated by adding the hourly ET_r values over the day of the image (Waters et al. 2002).

3. RESULTS AND DISCUSSION

Using SEBAL Algorithm or model various parameters value are found. The maximum value of Evapotranspiration was in 2010 and minimum in 2021 for wheat crop of 2A Distributary.

As shown in Table 1, 15 images from 2007 to 2021 were used. The values of the parameters obtained by the SEBAL algorithm for Wheat Crop are presented here. Surface Albedo (α) is taken 0.35%, the Normalized Difference Vegetation Index (NDVI) range between -1 to +1 and all the values comes under range, (T_s) is Surface Temperature in degree Celsius maximum surface temperature is 34.793 ($^{\circ}C$) in 2012 and

minimum in 2021 it was 23.806 ($^{\circ}C$), R_n is the net radiation flux at the surface (W/m^2) maximum R_n is 511.684 (W/m^2) in 2009 and the minimum is 97.253 (W/m^2) in 2020, (H) Sensible heat flux to the air (W/m^2) maximum H is 258.749 in 2009 and minimum is 64.923 in 2020, (G) is the Soil heat flux (W/m^2) maximum G is 91.303 in 2010 and the minimum is 11.653 in 2021, λET is Instantaneous value for the time of the satellite overpass (W/m^2) maximum λET is 187.759 in 2009 and minimum is 15.177 in 2020, ET_r is the Reference ET Fraction is maximum in 2017 (0.084) and minimum in 2015, 2018 (0.011), ET_{inst} is Instantaneous ET (mm/day) is maximum in 2009 (0.221) and minimum in 2020 (0.015), at the last ET_{24} (mm/day) are often more useful than instantaneous ET maximum in 2010 (4.476) and minimum in 2021 (0.645), all these value is obtained for the study area based on the studied methods. Map of the maximum and minimum Evapotranspiration are shown in Fig. 3.

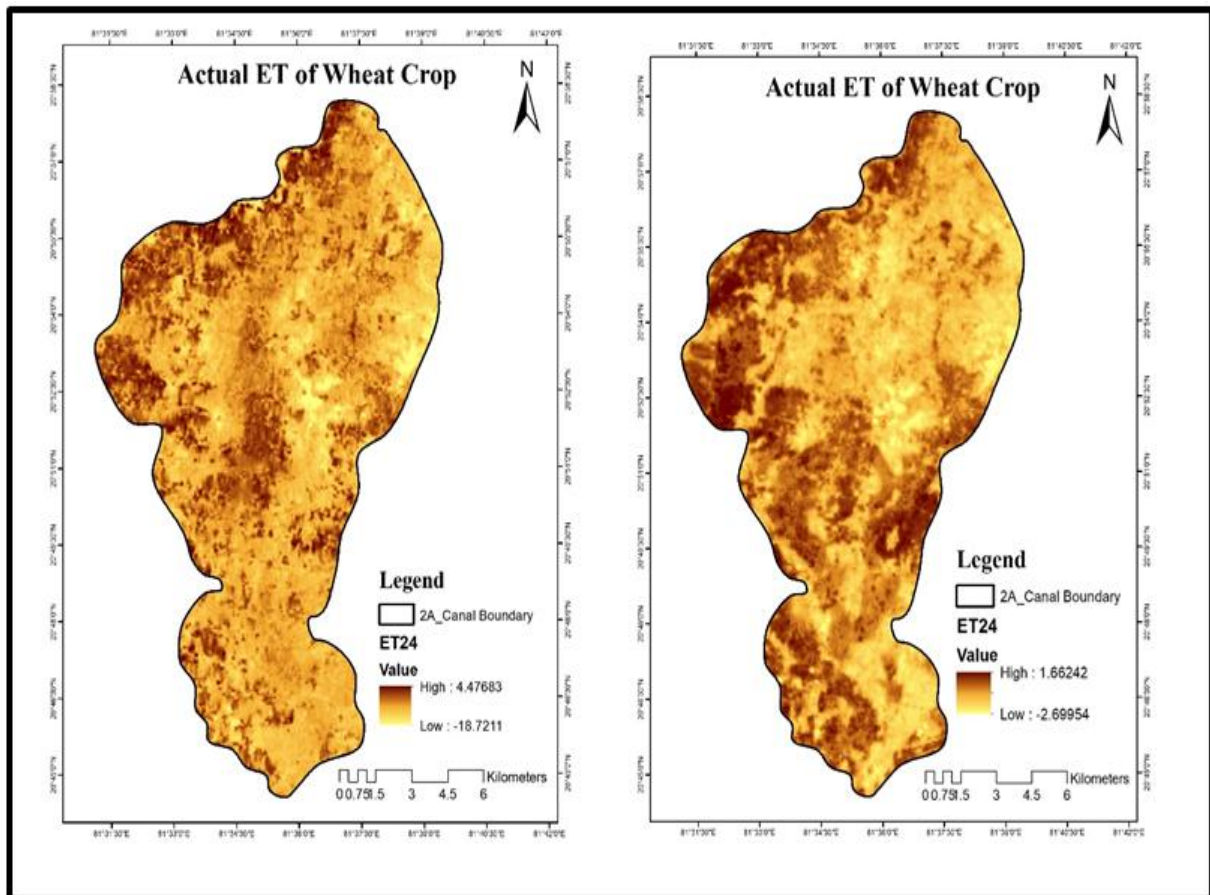


Fig. 3. Map showing maximum and minimum evapotranspiration

Table 1. The results from SEBAL model for wheat crop of Rabi season

Year	NDVI	Albedo %	T _s (c)	R _N (W/m ²)	H (W/m ²)	G (W/m ²)	λET (W/m ²)	ETrF	ETinst	ET ₂₄ (mm/day)
2007	0.103	0.35	27.853	387.971	215.887	47.756	124.327	0.062	0.183	4.144
2008	0.105	0.35	28.676	353.083	222.261	41.104	89.7184	0.057	0.164	3.185
2009	0.075	0.35	33.994	511.684	258.749	65.176	187.759	0.053	0.221	3.033
2010	0.106	0.35	30.058	395.456	197.648	91.303	106.505	0.048	0.124	4.476
2011	0.127	0.35	27.118	211.711	123.142	51.897	36.671	0.014	0.042	3.893
2012	0.118	0.35	34.793	343.434	173.502	81.281	88.651	0.037	0.104	3.131
2013	0.139	0.35	29.487	227.975	144.824	28.942	54.191	0.021	0.063	4.117
2014	0.262	0.35	27.598	203.358	134.803	25.959	42.596	0.017	0.049	2.928
2015	0.265	0.35	26.568	178.612	124.071	25.614	28.927	0.011	0.033	4.171
2016	0.205	0.35	26.804	231.291	151.073	18.696	61.522	0.027	0.071	2.828
2017	0.216	0.35	25.885	162.818	119.491	22.464	20.863	0.084	0.024	3.935
2018	0.207	0.35	29.731	167.418	118.094	24.578	24.746	0.011	0.028	4.111
2019	0.215	0.35	25.571	191.945	123.528	15.921	52.496	0.024	0.061	2.605
2020	0.228	0.35	25.198	97.253	64.923	17.153	15.177	0.061	0.015	2.645
2021	0.155	0.35	23.806	119.097	85.616	11.653	21.828	0.011	0.025	0.645

4. CONCLUSION

The increasing population and existing climate change scenario is posing a major challenge to the global freshwater resource. This challenge is more visible in agriculture sector, especially of water -stressed countries, as it is often the biggest user of freshwater supplies. Over the last few decades with the reduction of the water resources, India is facing critical problems with industrial and agricultural growth being impacted. Prediction of irrigation water demand involves computation of many water balance factors and evapotranspiration (ET) is one of its major components. ET is the combined loss of water from the soil as well as plants and it is a crucial component of the hydrologic cycle. The accurate estimation of crop evapotranspiration (ET_c) is vital in the management and development of water resources. The scarcity of freshwater resources or the misuse of water in agriculture has made the efficient and profitable use of water even more important.

The present study was carried out in Dhamtari district, Kurud block of Mahanadi Command area in Chhattisgarh State of Northern part of Dhamtari district. The area lies between $20^{\circ}.74'04''$ and $21^{\circ}.08'29''$ N latitudes and $81^{\circ}.47'50''$ and $81^{\circ}.85'30''$ E longitudes. To validate the outcomes from the SEBAL algorithm, FAO Penman-Monteith methods were employed to calculate the evapotranspiration values and evaluated using suitable performance metrics. The evaluation using SEBAL, along with the FAO-Penman-Monteith method, showed that SEBAL has a sufficient accuracy for estimating ET. The results showed that the SEBAL generated evapotranspiration values are in high agreement with the FAO Penman-Monteith method registering the highest correlation value ($R^2 = 0.826$) and the corresponding Root Mean Square Error was (RSME = 0.4386), Normalized Root Mean Square, (NRMSE= 0.386), Mean Absolute Error (MAE=1.17) and Nash Sutcliffe Efficiency (ENS = 0.843) for Wheat crop. In 2010 maximum ET_c and in 2021 minimum ET_c of wheat crop in the study area. We show that the results of this study can be applied in the studies of water resources management and appropriate irrigation management on farm level.

COMPETING INTERESTS

Authors have declared that no competing interests exist.

REFERENCES

1. Allen RG, Pereira LS, Raes D, Smith M. Crop evapotranspiration Guidelines computing crop water requirements. FAO Irrigation and drainage paper No. 56, FAO; 1998.
2. Ozturk F, Apaydin H. Estimating pan evaporation from limited meteorological observations from Turkey. *Water International*. 1998;23(3):184-189.
3. Bastiaanssen WGM, Noordman EJM, Pelgrum H, Davids G, Thoreson BP, Allen RG. SEBAL model with remotely sensed data to improve water-resources management under actual field conditions. *Journal of Irrigation and Drainage Engineering*. 2005;131(1):85-93.
4. Lou BS, Rajaji U, Chen SM, Chen TW. A simple sonochemical assisted synthesis of NiMoO₄/chitosan nanocomposite for electrochemical sensing of amlodipine in pharmaceutical and serum samples. *Ultrasonics Sonochemistry*. 2020;64: 104827.
5. Yamaç SS. Artificial intelligence methods reliably predict crop evapotranspiration with different combinations of meteorological data for sugar beet in a semiarid area. *Agricultural Water Management*. 2021;254:106968.
6. Goyal MR, Harmsen EW. eds., *Evapotranspiration: principles and applications for water management*. CRC Press; 2013.
7. Shabani S, Samadianfard S, Sattari MT, Mosavi A, Shamshirband S, Kmet T, Várkonyi-Kóczy AR. Modeling pan evaporation using Gaussian process regression K-nearest neighbors random forest and support vector machines; comparative analysis. *Atmosphere*. 2020;11(1):66.
8. Sattari K, Rahbar N, Ahadi M, Haghani H. The effects of a temporal processing-based auditory training program on the auditory skills of elderly users of hearing aids: a study protocol for a randomized clinical trial. *F1000Research*. 2020;9.
9. Valayamkunnath P, Sridhar V, Zhao W, Allen RG. Intercomparison of surface energy fluxes, soil moisture, and evapotranspiration from eddy covariance, large-aperture scintillometer, and modeling across three ecosystems in a semiarid climate. *Agricultural and Forest Meteorology*. 2018;248:22-47.

10. Sattari SZ, Bouwman AF, Giller KE, van Ittersum MK. Residual soil phosphorus as the missing piece in the global phosphorus crisis puzzle. Proc. Natl. Acad. Sci. U. S. A. 2012;109(16): 6348–6353.
11. Sattari MT, Apaydin H, Shamshirband S. Performance Evaluation of Deep Learning-Based Gated Recurrent Units (GRUs) and Tree-Based Models for Estimating ETo by Using Limited Meteorological Variables. Mathematics. 2020;8(6):972. Available:<https://doi.org/10.3390/math8060972>
12. Rawat J, Saxena J, Sanwal P. Biochar: a sustainable approach for improving plant growth and soil properties. Biochar-an Imperative Amendment for Soil and the Environment. 2019;1-17.
13. Allen RG, Tasumi M, Trezza R. Satellite-based energy balance for mapping evapotranspiration with internalized calibration (METRIC)—Model. Journal of Irrigation and Drainage Engineering. 2007;133(4):380-394.
14. Seneviratne SI, Lüthi D, Litschi M, Schär C. Land-atmosphere coupling and climate change in Europe. Nature. 2006 Sep 14;443(7108):205-9.
15. Bashir M, Afzal MT, Azeem M. Reliability and validity of qualitative and operational research paradigm. Pakistan journal of statistics and operation research. 2008 Jan 1:35-45.
16. Qiu X, Mao Q, Tang Y, Wang L, Chawla R, Pliner HA, Trapnell, C. Reversed graph embedding resolves complex single-cell trajectories. Nature methods. 2017;14(10): 979-982.

© 2023 Dhruw et al.; This is an Open Access article distributed under the terms of the Creative Commons Attribution License (<http://creativecommons.org/licenses/by/4.0>), which permits unrestricted use, distribution, and reproduction in any medium, provided the original work is properly cited.

Peer-review history:

*The peer review history for this paper can be accessed here:
<https://www.sdiarticle5.com/review-history/103419>*